17th Australasian Fluid Mechanics Conference
Auckland, New Zealand
5-9 December 2010

Natural convection flows in reservoir sidearms using Large Eddy Simulation and an Immersed Boundary Method

K. A. Dittko[1], M. P. Kirkpatrick[1] and S. W. Armfield[1]

[1]School of Aerospace, Mechanical and Mechatronics Engineering
University of Sydney, NSW 2006, Australia

Abstract

Numerical simulation was conducted of turbulent natural convection in domains representing the sidearm of a lake or water reservoir. Lateral temperature gradients exist due to the varying depth of the cavity, resulting in lateral circulation. These flows are important in a reservoir as they can carry with them particles and various pollutants, transporting and mixing them with the central section. Therefore study in this area is important in water quality management.

The domains studied include a two-dimensional triangular cavity as well as more realistic three-dimensional setups. Heat input is through a solar radiation model consisting of a heat flux from the sloped bottom boundaries as well as an internal heating source term in the body of the water. The heat flux at the bottom boundary induces natural convection including convective plumes and a large scale circulation, while the internal heating acts to stabilise the flow through the generation of a stable density stratification.

The simulations use a Cartesian grid with an Immersed Boundary Method (IBM) for sloped surfaces on the bottom and sides. The IBM involves using forcing terms in the flow equations to represent a surface. This surface may fall anywhere within a computational cell, so there is no requirement for the grid to be aligned with the surface. Other approaches commonly used include cut cells for Cartesian grids, body fitted coordinates, and unstructured meshes. The IBM has the advantage of greatly simplifying grid generation and boundary condition implementation, while still being less computationally expensive than the alternatives.

Introduction

The problem of a reservoir sidearm has received only limited attention in the literature. Some examples are [4, 5, 6, 8]. These include scaling analysis and numerical simulation, but always for a simple two-dimensional triangular domain. This simplification is a good approximation for the shallow near-shore region of some reservoirs, in particular natural lakes, where the shoreline is quite straight, however it ignores the three-dimensional flow effects.

This paper aims to extend this work to a more realistic sidearm, as is quite common in man-made reservoirs. These sidearms are narrow sections formed when a river is dammed and an area flooded. The two-dimensional triangle is no longer representative, but rather a tetrahedron is a better approximation. This tetrahedron is not regular, and does not have a base as such. Rather one face is horizontal at the top, the reservoir surface, and one face is vertical, representing the interface between the sidearm and the main reservoir body.

Method

Figure 1 shows the setup of the computational domain. An important feature of this problem is that the heating is modelled as a solar flux at the surface. The radiation is gradually absorbed as it penetrates the water, thus providing an internal heating source. The intensity of the radiation will decrease with depth, as described by Beers Law (see for example [9]). Lei *et al* [5] approximate the attenuation coefficient as having a single value across all wavelengths, so the source term for internal heating in the cavity is

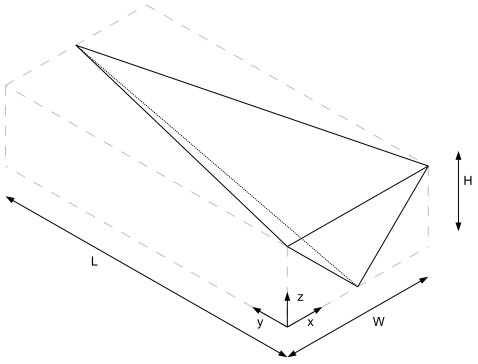

Figure 1: This figure shows the domain and coordinate axes for a tetrahedron representing a reservoir sidearm. In reality the full computational domain would be a few cells larger than shown to accommodate the Immersed Boundary ghost cells.

$$S = H_0 \eta e^{\eta z}, \tag{1}$$

where H_0 is the surface heating intensity, z is the negative distance through which the radiation has travelled, and η is the attenuation coefficient.

This means that the heating intensity close to the surface will be greater. Since it is not horizontally dependent, this input will not cause any lateral temperature gradient and therefore will not induce circulation in the cavity. This internal heating will actually work to form a stably stratified temperature structure.

In shallow areas some of the radiation will penetrate the entire depth of the water, heating the bottom surface and consequently heating the bottom fluid layer. It is for this reason that the shallow section of a reservoir is interesting. The thermal boundary layer formed at the bottom surface does induce instability in the flow, and is also horizontally dependent.

The boundary condition at the bottom of the cavity is modelled in [5] as a constant flux

$$\frac{\partial T}{\partial \hat{n}} = -\frac{1}{k} H_0 e^{\eta z}, \tag{2}$$

which assumes that all radiation reaching the surface is absorbed and the boundary is insulated on the external side. In Equation 2, $\hat{n}$ is the direction normal to the boundary and k is the thermal diffusivity.

The result is that there are effectively two competing heat sources. The bottom surface heat flux is acting to drive a circulation in the cavity, while the radiation absorption which is

greatest near the top is acting to stabilise the water. At moderate Rayleigh numbers this results in a bulk flow up along the bottom surfaces toward the tip and out along the top.

The boundary conditions at the end wall are non-slip ($u = v = w = 0$), while the top surface is stress-free ($\frac{\partial u}{\partial z} = 0, \frac{\partial v}{\partial z} = 0, w = 0$). The end wall is insulated, as is the top surface, since it is assumed any heat loss or gain through the surface is small when compared with the radiation absorption. This is also consistent with the 2D triangle simulations in the literature [5, 1].

One issue here is that over time the average temperature will continue to rise since there are no heat sinks. The simulation will reach a quasi-steady state, however, where the temperature over the whole cavity is rising at the same rate.

Numerical Method

The original solver used was developed and validated by Kirkpatrick *et al* [2, 3]. It uses a finite volume, fractional step, pressure correction method. The code solves the Navier-Stokes equations using a 4th order Central Difference scheme for momentum, 4th order Central Difference scheme with ULTRA flux limiter [7] for scalars and is 2nd order accurate in time.

The solver has been modified to include an Immersed Boundary Method. The method used for the IBM is based on [10] and [11], and these papers contain a more comprehensive description of the procedure. The IBM involves the addition of an extra term to the momentum equations $\mathbf{f_m}$, and an extra term to the energy equation f_e, so the equations solved become

$$\nabla \cdot \mathbf{u} = 0, \tag{3}$$

$$\frac{\partial \mathbf{u}}{\partial t} + \mathbf{u} \cdot \nabla \mathbf{u} = -\frac{1}{\rho_{ref}} \nabla P + \frac{\rho - \rho_{ref}}{\rho_{ref}} \mathbf{g} + \nu \nabla^2 \mathbf{u} + \mathbf{f_m}, \tag{4}$$

$$\frac{\partial T}{\partial t} + \mathbf{u} \cdot \nabla T = \frac{\nu}{Pr} \nabla^2 T + f_e. \tag{5}$$

The process for determining the forcing terms involves firstly using a bi-linear interpolation method to calculate actual values on the virtual boundary. The advantage of using the IBM is that this virtual boundary does not need to coincide with a grid point. These actual values on the virtual boundary are then compared to the desired value at that location. From this difference the forcing term is calculated, acting to drive the actual value toward the desired value.

In the case of Dirichlet boundary conditions the desired velocities and desired temperatures are set to a constant value. For a Neumann boundary condition an extra layer of virtual nodes is created a small distance inside the immersed boundary nodes so that each node on the boundary has a corresponding node in the flow. The desired temperature is then calculated at each timestep using the extra nodes in the flow in order to give the desired temperature gradient at the boundary.

Results

The simulations shown are for a grid of $320 \times 80 \times 40$ cells. The aspect ratio for the height of the cavity versus the length is $A_L = H/L = 0.14$ and the aspect ratio for the height versus the half-width is $A_W = 2H/W = 1$. The purpose of the simulations is to look at the shallow edge section of a reservoir, so the maximum depth has been set to $H = \eta^{-1}$, meaning there will be appreciable radiation penetrating the full depth at all but the deepest parts of the cavity. The critical parameters in this flow are the Prandtl and Grashof numbers which are given respectively by

$$Pr = \frac{\nu}{k}, \tag{6}$$

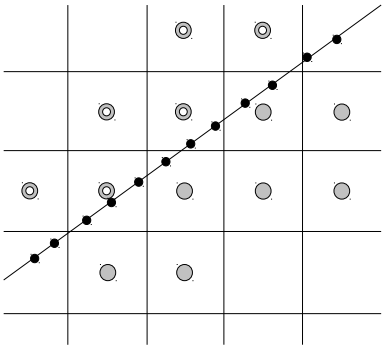

Figure 2: Diagram showing the grid in the vicinity of the Immersed Boundary. The small black circles are the virtual boundary points and have coordinates $\mathbf{x}_s$. The large filled circles below the virtual boundary represent points on the computational grid outside the flow where the forcing functions are applied. The large rings on the other side of the boundary are in the flow, meaning the forcing function is not applied, but they are used to calculate the properties at the virtual boundary points.

$$Gr = \frac{g\beta H_0 H^4}{\nu^2 k}. \tag{7}$$

In all results presented here the Prandtl and Grashof numbers are kept constant at $Pr = 7.0$ and $Gr = 1.3 \times 10^4$, with the exception of Figure 8 which has a higher Grashof number of $Gr = 5.8 \times 10^5$. At the lower Gr value the flow is not yet turbulent. The apparent fluctuations close to the boundary seen in Figure 6 are actually just an idiosyncrasy of the visualisation.

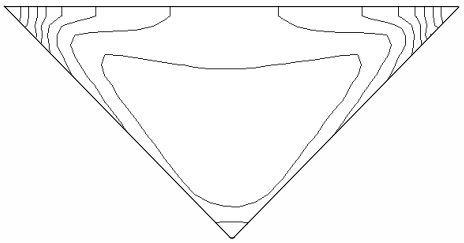

Figure 3: Contour plot of temperature on a 2D cross section near the deep end of the cavity, taken through $y = \frac{1}{8}L$. Intervals are 0.1 non-dimensional temperature units, with the maximum near the top left and top right corners.

Discussion

Cross sections of the flow, taken perpendicular to the y axis, remain similar in appearance for the length of the cavity. Contour and vector plots taken toward the deep end of the cavity are shown in Figures 3 and 4. A very strong flow up the sloped sides, across the top and down the centre is evident in the vector plot. The temperature contours show that while the temperature gradient is greatest near the top corners, there is significant heat transport along the surface away from the top corners. This flow is symmetric about the centreline, and each half is quite similar to the flow seen in 2D simulations of a triangular cavity [5].

In contrast, cross sections showing flow along the length of the cavity are much different. In Figure 6 we see that the flow is similar near the tip, however Figure 5 shows that for most of

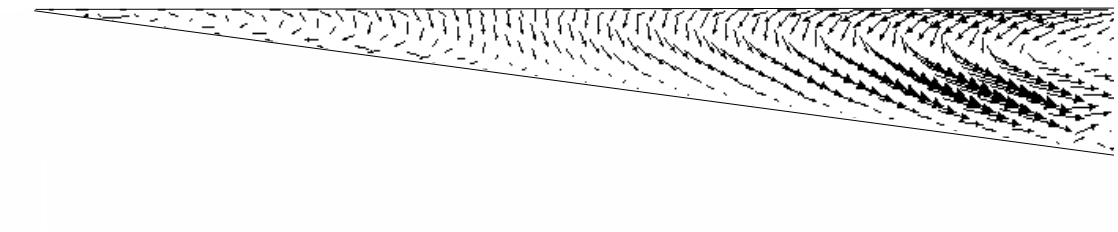

Figure 5: Velocity vector plot on a 2D cross section along the cavity centreline, through $x = \frac{1}{2}W$. Flow at the deep end is down the slope at the bottom and towards the shallow end at the top, while the opposite flow exists close to the shallow end.

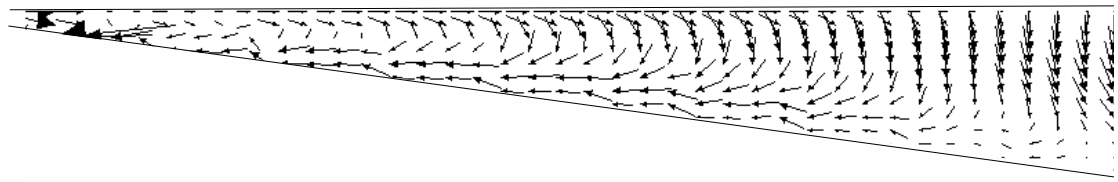

Figure 6: Vector plot zoomed in on the tip, from $y = L$ to $y = \frac{1}{2}L$, along the cavity centreline at $x = \frac{1}{2}W$. This figure more clearly shows the flow up the bottom slope and out along the top.

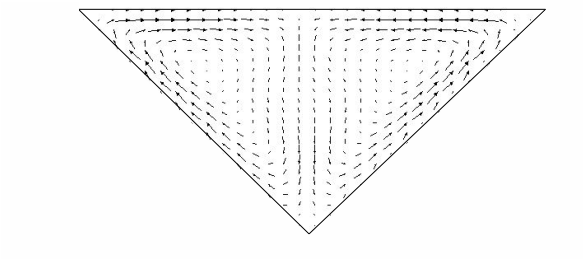

Figure 4: Velocity vectors on a 2D cross section near the deep end of the cavity, taken through $y = \frac{1}{8}L$

the domain the flow is actually down the slope, the opposite to what is seen in the flow across the cavity or in simulations of a 2D triangular domain. Overall though the flow across the domain dominates, resulting in a much weaker flow field in planes perpendicular to the x axis.

Figure 7 shows a large horizontal temperature gradient close to the shallow tip of the cavity, with very small gradient past about $y = \frac{3}{4}L$. This shows that there is low heat transport away from the shallow end of the cavity, which supports what is shown in the vector plots. In 2D triangular cavity simulations we see a strong flow away from the tip along the surface, which allows for much higher heat transport away from the tip resulting in a relatively consistent temperature gradient over the length of the cavity. This outflow near the surface is not seen, giving the reduced heat transport that is suggested by the temperature contour plot.

Figures 5 and 6 show a clear distinction between the flow at the shallow and deep ends of the cavity. With little interaction between the two sections, the result is that the shallow end becomes significantly warmer than the deep end as seen in Figure 7 as there is no mechanism for the heat to be transported away.

Figure 8 is the only plot shown with higher Grashof number $Gr = 5.8 \times 10^5$. This vector plot shows turbulent convection developing particularly towards the deep end of the cavity. This is in agreement with [8] where it was shown that turbulent convection at higher Gr develops first near the deep end with stable convection and conduction remaining near the shallow tip. Despite this agreement in terms of transition to turbulence, there still appears to be much less mixing between the shallow region and the deeper parts of the cavity.

Conclusions

Reservoir sidearm simulations have been conducted for a three-dimensional cavity. Some significant differences were seen between this case and the simple two-dimensional triangle as presented in the literature. The transition to turbulence was similar, however differences exist in particular in that the current work shows much less flow away from the shallow part of the domain. This means that in a real world situation with similar geometry to the simulations the mixing between the sidearm and the main reservoir body would be much less than anticipated from looking at 2D simulations. This is significant, as the mixing would include not only temperature but also pollutants, nutrients and micro-organisms.

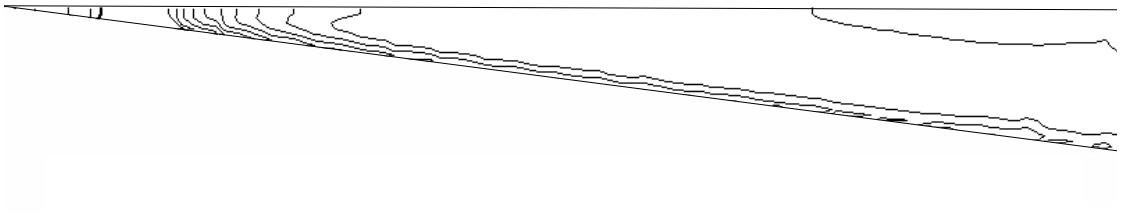

Figure 7: Temperature contours on a 2D cross section along the cavity centreline, through $x = \frac{1}{2}W$. Intervals are 0.1 non-dimensional temperature units, with the maximum at the top left corner.

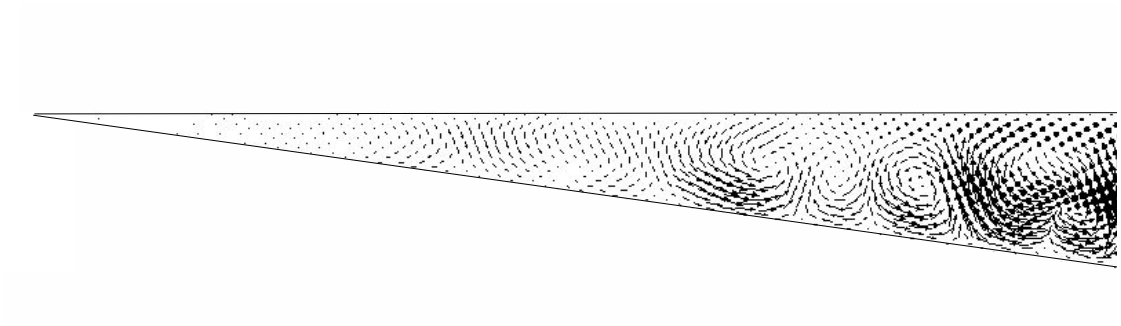

Figure 8: $Gr = 5.8 \times 10^5$. Vector plot 2D cross section along the cavity centreline, through $x = \frac{1}{2}W$. Turbulent convection can be seen developing toward the deep part of the cavity.

References

[1] Farrow, D. E. and Patterson, J. C., The daytime circulation and temperature structure in a reservoir sidearm, *International Journal of Heat and Mass Transfer*, **37**, 1994, 1957–1968.

[2] Kirkpatrick, M. P. and Armfield, S. W., Experimental and large eddy simulation results for the purging of salt water from a cavity by an overflow of fresh water, *International Journal of Heat and Mass Transfer*, **48**, 2005, 341–359.

[3] Kirkpatrick, M. P., Armfield, S. W. and Kent, J. H., A representation of curved boundaries for the solution of the navier-stokes equations on a staggered three-dimensional cartesian grid, *Journal of Computational Physics*, **184**, 2003, 1–36.

[4] Lei, C. and Patterson, J. C., Natural convection in a reservoir sidearm subject to solar radiation: experimental observations, *Experiments in Fluids*, **32**, 2002, 590–599.

[5] Lei, C. W. and Patterson, J. C., Unsteady natural convection in a triangular enclosure induced by absorption of radiation, *Journal of Fluid Mechanics*, **460**, 2002, 181–209.

[6] Lei, C. W. and Patterson, J. C., A direct stability analysis of a radiation-induced natural convection boundary layer in a shallow wedge, *Journal of Fluid Mechanics*, **480**, 2003, 161–184.

[7] Leonard, B. P. and Mokhtari, S., Beyond first-order upwinding: The ultra-sharp alternative for non-oscillatory steady-state simulation of convection, *International Journal for Numerical Methods in Engineering*, **30**, 1990, 729–766.

[8] Mao, Y. D., Lei, C. W. and Patterson, J. C., Unsteady natural convection in a triangular enclosure induced by absorption of radiation - a revisit by improved scaling analysis, *Journal of Fluid Mechanics*, **622**, 2009, 75–102.

[9] Rabl, A. and Nielsen, C. E., Solar ponds for space heating, *Solar Energy*, **17**, 1975, 1–12.

[10] Zhang, N. and Zheng, Z. C., An improved direct-forcing immersed-boundary method for finite difference applications, *Journal of Computational Physics*, **221**, 2007, 250–268.

[11] Zhang, N., Zheng, Z. C. and Eckels, S., Study of heat-transfer on the surface of a circular cylinder in flow using an immersed-boundary method, *International Journal of Heat and Fluid Flow*, **29**, 2008, 1558–1566.